

Isostasy of the Moon from high-resolution gravity and topography data: Implication for its thermal history

T. Sugano

Division of Earth and Planetary Sciences, Kyoto University, Kyoto, Japan

K. Heki

Division of Earth and Planetary Sciences, Hokkaido University, Sapporo, Japan

Received 22 November 2004; accepted 9 December 2004; published 31 December 2004.

[1] The Lunar Prospector line-of-sight acceleration data after terrain correction have been inverted to the high-resolution Bouguer gravity anomalies of the lunar nearside. Lithospheric thicknesses of the early Moon were investigated by comparing the gravity anomalies of craters and impact basins of various dimensions. The lithosphere was already thick enough to support craters with diameters up to 300 km in the Pre-Nectarian and Nectarian Periods. Degree of isostatic compensation of larger impact basins suggested lithospheric thickness of 20–60 km at that time, which depended more on localities rather than age differences. *INDEX TERMS:* 1221 Geodesy and Gravity: Lunar geodesy and gravity (6250); 5430 Planetology: Solid Surface Planets: Interiors (8147); 5455 Planetology: Solid Surface Planets: Origin and evolution. **Citation:** Sugano, T., and K. Heki (2004), Isostasy of the Moon from high-resolution gravity and topography data: Implication for its thermal history, *Geophys. Res. Lett.*, 31, L24703, doi:10.1029/2004GL022059.

1. Introduction

[2] Gravity data are useful to infer internal structures of rocky planets/satellites. Such data have been obtained by tracking artificial satellites because spherically asymmetric gravity fields let their orbital elements evolve in time. The Lunar Prospector (LP) was launched on 7 January 1998 [Binder, 1998]. The LP carried out a half-year extended mission with an average altitude of 30 km after its one-year nominal mission.

[3] Using the Doppler tracking data, Konopliv *et al.* [2001] modeled the lunar gravity potential as spherical harmonic coefficients (Stokes' coefficients) complete to 165th degree/order (LP165P). Unlike other celestial bodies, direct radio tracking of a lunar low orbiter is impossible on its farside because of the synchronous rotation of the Moon. To estimate the Stokes' coefficients with a non-global data set, one must regularize the normal equation using e.g., the Kaula's rule [Kaula, 1963]. Apart from the gravity model, Sugano and Heki [2004] performed direct inversion of LP line-of-sight acceleration (LOSA hereafter) data into high-resolution free-air gravity anomalies of the lunar nearside (see R. A. Simpson, Software interface specification for the line of sight acceleration profile data record (LOSAPDR), available at http://pds-geosciences.wustl.edu/geodata/lp-l-rss-5-los-v1/lp_1103/document/losapdr.txt, for detailed procedure to calculate LOSA from the Doppler tracking data).

[4] By combining surface topography and gravity data, one can infer Moho irregularity and degree of isostatic compensation [Neumann *et al.*, 1996; Arkani-Hamed, 1998; Wieczorek and Phillips, 1999; Reindler and Arkani-Hamed, 2001]. This, in turn, provides information on the flexural rigidity of the lunar lithosphere. Because the lunar lithospheric thicknesses have been increasing monotonously throughout its cooling history [Spohn *et al.*, 2001], substantial parts of the isostatic response are considered to have occurred in short periods after the formation of surface structures. Thus we can infer ancient lithospheric thickness by studying the lunar isostasy, and this would provide a unique constraint on the early thermal history of the Moon.

2. Bouguer Gravity Anomaly

2.1. Terrain Correction

[5] Large parts of short-wavelength gravity anomalies come from the surface topography. Their contributions can be calculated if the topography and crustal densities are known. To perform terrain correction for the LOSA data, we used the Clementine laser altimetry grid data, with an apparent resolution as high as $0.25^\circ \times 0.25^\circ$.

[6] For the density structure of the lunar crust, Wieczorek and Phillips [1998] compared several different models. They concluded that only single-layered crust with a uniform density and dual-layered crust with variable upper/lower crustal thicknesses give physically meaningful results. In the present study, however, the difference between the two models is not important because depths of craters (up to 4 km) are much less than the thickness of the upper crust in the dual-layered model (~ 30 km). So we simply assumed uniform crustal density of $2,900 \text{ kg m}^{-3}$.

[7] Positive (negative) gravitational acceleration due to mass excess (deficit) at a certain point of the lunar surface can be inferred from height difference from reference surface. At a certain satellite position where the LOSA was measured, we calculated acceleration vectors using the surface height data at all the grid points of the Moon. Then their projections to instantaneous line-of-sight direction were integrated over the lunar surface to obtain contribution of the entire lunar surface topography to particular LOSA. Then the contribution is subtracted from the raw LOSA. Figure 1 shows an example of LOSA profiles before and after this correction for a certain path above the Copernicus crater (93 km in diameter).

[8] The LOSA data after the terrain correction were processed using exactly the same least-squares method that

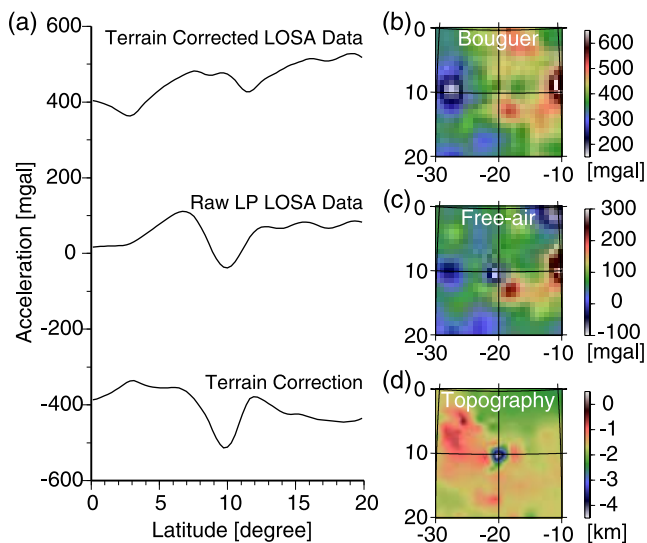


Figure 1. (a) Example of the terrain correction around the Copernicus crater. Line-of-sight gravity component comes from surface topography (bottom) are subtracted from raw LP LOSA (middle) to obtain terrain-corrected LOSA (top). To the right are shown (b) the Bouguer anomalies estimated using the terrain-corrected LOSA data, (c) free-air anomalies estimated using the raw LOSA data, and (d) topographic map.

Sugano and Heki [2004] used to obtain the free-air anomaly (i.e., direct estimation of mass distribution on the lunar reference surface). No artificial constraints were introduced to stabilize the inversion in the method. We tested if the same method works well in estimating excess masses at Moho (~ 40 km deep) using synthesized data in a way similar to *Sugano and Heki* [2004]. The test recovery resulted in slight underestimation of the excess mass there. However, it was $\sim 10\%$ at most, and would not affect our final discussion of lithospheric thicknesses. The obtained gravity anomaly corresponds to the Bouguer anomaly in terrestrial gravity studies because they reflect mainly subsurface density structures. The maximum resolution of this map is 24 km, equivalent to spherical harmonics complete to 225th degree/order. But the actual resolution could be worse where topographic resolutions are coarse.

2.2. Mare Mass Correction

[9] The assumption of uniform crustal density in deriving the Bouguer anomalies is inappropriate at the lunar maria where basalt layers ($3,300 \text{ kg m}^{-3}$) are significantly denser than average highland crust ($2,900 \text{ kg m}^{-3}$). They tend to enhance positive Bouguer anomalies, and let us overestimate the sizes of mantle plugs (Moho uplifts) beneath them. We evaluated the mass excesses of the mare basalts for nine major mascons (Crisium, Grimaldi, Humorum, Imbrium, Nectaris, Orientale, Schiller-Zucchius, Serenitatis and Smythii) and removed them to isolate the gravity signals of the Moho undulations.

[10] Gravity anomalies due to the excessive density of the maria were calculated using the Parker's algorithm [Parker, 1972; Neumann et al., 1996]. In using this algorithm, 1-dimensional FFT is employed, and the density contrast of 400 kg m^{-3} is assumed. Recently, diameter-

depth relationship for major basins were reanalyzed using the Clementine altimetry data set, and revised estimates of the mare basalt thicknesses were reported [Williams and Zuber, 1996] except for the Schiller-Zucchius basin, whose mare thickness we estimated using these new parameters.

[11] Some kinds of tectonic features in maria also reflect subsurface structures. Concentric cylindrical shapes of the mare basalt for the major mascon basins were suggested by studying orientations of linear and arcuate rills and ridges on their surface [Solomon and Head, 1980]. In this model, basalt layers are thicker at basin centers than those based on the new Clementine data. To take the new results into account, we revised the cylindrical model by adjusting the maximum basalt thicknesses to those from the Clementine data [Wieczorek and Phillips, 1998].

[12] The mare mass correction was the largest for the Imbrium basin, 95.8 mgal and this corresponds to 17% of its Bouguer anomaly. In spite of small sizes, Grimaldi, Humorum and Schiller-Zucchius needed relatively large corrections. The correction for the Orientale basin was only 6.3 mgal reflecting its thin mare fill. Such corrections were subtracted from the Bouguer anomalies at individual grid points. The corrected anomaly map is shown in Figure 2.

3. Lithospheric Thickness

[13] To quantify degree of isostatic compensation of craters, we calculate their mass deficits (lacks of mass responsible for negative gravity anomalies of the craters relative to background values) using our Bouguer anomaly maps as was done with the free-air anomalies of *Sugano and Heki* [2004].

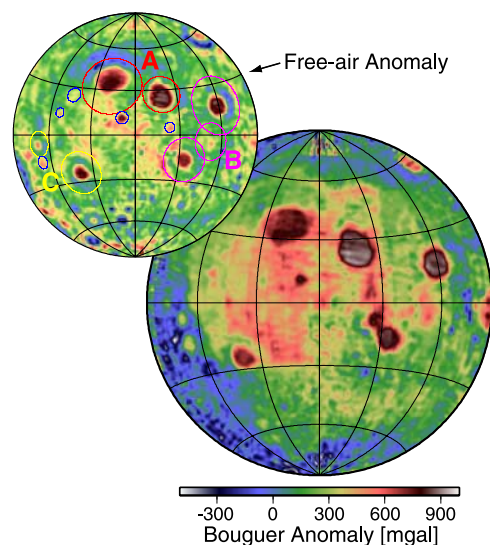


Figure 2. Bouguer anomaly map obtained from the LP LOSA data and the Clementine grid topography data. We assumed uniform crustal density of $2,900 \text{ kg m}^{-3}$, with additional correction for the excess density of mare basalts. Free-air anomalies by *Sugano and Heki* [2004] are also shown for comparison. Colored circles on the free-air anomaly are mascon groups shown in Figure 3c. Blue circles are positive anomalies without conspicuous basin topographies (possibly of volcanic origin).

[14] Because the average resolution of topographic measurement by the Clementine laser altimeter was ~ 100 km along-track and ~ 60 km across-track [Smith *et al.*, 1997], we only used medium-sized craters (60–300 km in diameter) which have sufficient number of actual altimetry footprints in and around them. Figure 3 compares the mass deficits of such craters in the two gravity anomaly maps. Size-dependent mass deficits in the free-air anomalies simply reflect topographic lows of the craters [Sugano and Heki, 2004]. In the Bouguer anomalies, one can see such mass deficits mostly disappear. This indicates that the Moho is flat beneath them (i.e., isostatically uncompensated). The sizes of the circles show the ages of the craters, that is, a larger symbol denotes a younger age. No clear correlation seems present between the compensation state and the age of the craters.

[15] In order to constrain lithospheric thicknesses, we examine the development of mantle plugs for larger topographic features such as mascon basins (200–1,000 km in diameter). We discuss the mass deficits of mascons shown in Figure 3c (their “deficits” are negative because of mantle plugs, that is, they are mass excesses actually, but we use the same term for simplicity), using the mare-mass-

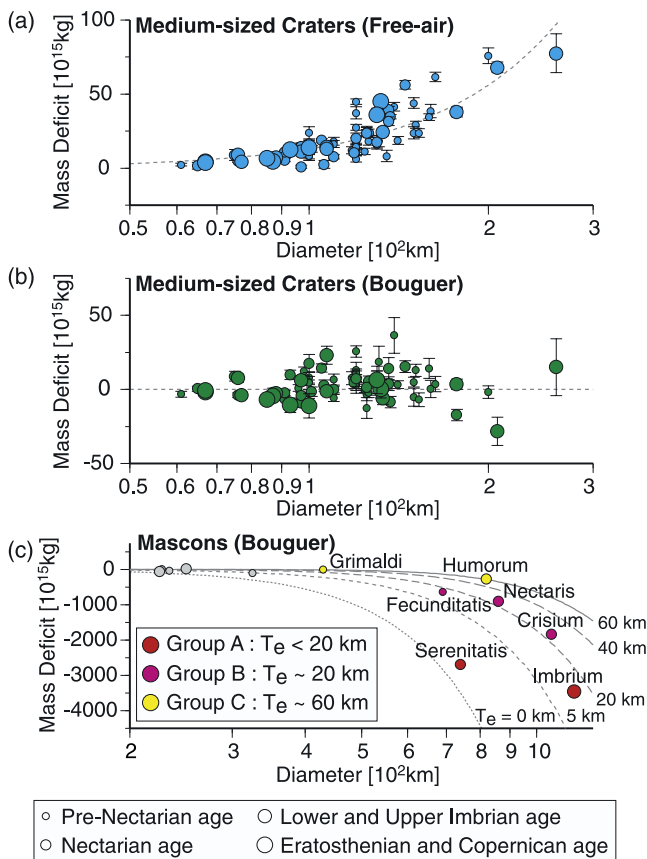


Figure 3. The mass deficits of medium-sized craters obtained from (a) free-air and (b) Bouguer anomalies. Dashed curves are the mass deficits expected when no isostatic compensation occurred. (c) The observed mass deficits of mascon basins and those expected for various lithospheric thickness. Mascons greater than 400 km are classified into three groups by lithospheric thickness. The sizes of circles denote ages of the craters.

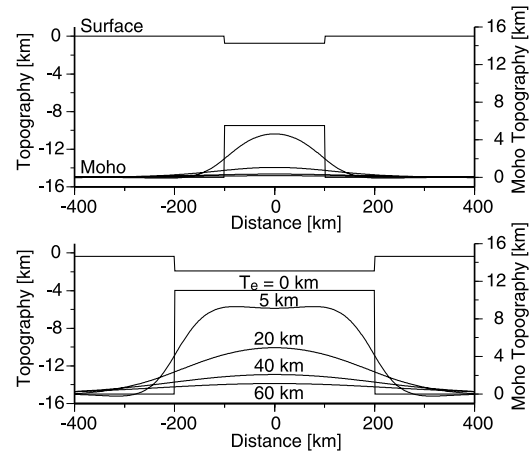


Figure 4. Moho topography model. The development of the mantle plug (Moho uplift) depends on the crater sizes and lithospheric thicknesses.

corrected Bouguer anomalies obtained in the previous section.

[16] Isostatic compensation model of an elastic spherical shell for the Moon is given by Turcotte *et al.* [1981]. Surface topography $H(\theta, \phi)$ can be expressed as the sum of spherical harmonics with coefficients H_{nm} (n -th degree, m -th order). Isostatic compensation is suppressed for short wavelength components due to lithospheric rigidity, resulting in the degree-dependent relationship between the surface H_{nm} and the Moho W_{nm} topographies [Arkani-Hamed, 1998],

$$W_{nm} = -\frac{\rho_c}{\Delta\rho} \frac{1}{\xi_n} H_{nm}, \quad (1)$$

where

$$\xi_n = \frac{Dn^2(n+1)^2}{R^4\Delta\rho g_m} + \frac{ET_e}{R^2\Delta\rho g_m} + 1 \quad (2)$$

and

$$D = \frac{ET_e^3}{12(1-\nu^2)}. \quad (3)$$

The crustal density ρ_c and density contrast at Moho $\Delta\rho$ are taken as $2,900 \text{ kg m}^{-3}$ and 400 kg m^{-3} , respectively. g_m and R are the gravitational acceleration and radius of the Moon. D is the flexural rigidity of the lithosphere, and T_e is the lithospheric thickness. The Young's modulus E and Poisson's ratio ν are assumed 10^{11} Pa and 0.25 , respectively. We assumed crater depths is proportional to $3.8 \times 10^{-3}d^{1.0}$, where d is the diameter [after Dehon and Waskom, 1976]. The basin topography was expanded with the spherical harmonics H_{nm} complete to 2,000th degree/order. Next, the Moho topography W_{nm} was calculated using equations (1)–(3). Then the W_{nm} was converted back to space domain $W(\theta, \phi)$. The development of mantle plugs is controlled by the dimension of surface topography and lithospheric thickness (Figure 4). The volume of the mantle plug was multiplied by the density contrast to obtain the

mass deficit (mass excess, if negative), as shown by curves in Figure 3c.

[17] Figure 3c shows the Serenitatis basin has achieved almost complete isostatic compensation (Airy compensation), that is, lithosphere beneath it is very thin, say $T_e < 5$ km. For other basins, however, there seems no simple correlation between the size and lithospheric thickness. From Figure 3c, we can see the thicknesses were in a range 20–60 km when they were formed (i.e., Pre-Nectarian to Nectarian period, 0–0.8 Gyr after the lunar formation).

4. Discussion and Conclusion

[18] Using our high-resolution Bouguer gravity anomaly map, we investigated isostatic compensation states of the lunar craters. The absence of mass deficits of the medium-sized craters in the Bouguer anomalies indicates no isostatic compensation has occurred for those with diameters up to 300 km. This suggests that lithosphere of a certain thickness had been already present when these craters were formed.

[19] This conclusion is somewhat different from *Reindler and Arkani-Hamed* [2001], who studied compensation states of 49 intermediate-sized craters (120–600 km in diameter) using the LP165P model truncated at 110th degree/order. They calculated mass anomalies of craters by subtracting the mass required for the isostatic compensation of the surface topography from the total mass, and concluded that majority of the craters indicate some degrees of compensation. Such a difference is considered to have come from gravity model difference, that is, they used the LP165P whose short-wavelength noises are larger than our model as *Sugano and Heki* [2004] demonstrated with the mass deficit residuals of craters around the best-fit curve. It might be also due to their inclusion of farside craters, whose gravity anomalies are less reliable.

[20] We evaluated compensation states of larger impact basins to constrain the lithospheric thickness. We compared the mass deficits (excesses) in the Bouguer anomalies with the isostatic compensation model. The lithosphere was inferred to be as thick as 20–60 km during the Pre-Nectarian to Nectarian period. Lunar thermal evolution has been numerically investigated assuming various initial magma ocean depths [*Spohn et al.*, 2001]. The lithospheric thickness inferred in the present study may provide a new constraint to promote realistic simulation studies.

[21] The lithosphere beneath the Serenitatis basin was found to be thinner than other regions. The origin of this basin is a matter of debate. The Imbrian grooves and the thorium anomaly within the South Pole-Aitken, together with a model calculation of impact ejecta, let *Wieczorek and Zuber* [2001] propose that the basin was formed by a single oblique impact. On the other hand, based on photogeological studies, *Scott* [1974] suggested the basin was formed by double impact. If 10% of the kinetic energy of an impacting body were converted into heat, impact of a 45 km diameter body with velocity 20 km s⁻¹ could increase the temperature of the lunar surface layer down to depth of 50 km by 400 K. The base of the lithosphere is considered to be ~1070 K isotherm, beneath which mantle convection occurs [*Stevenson et al.*, 1983]. The hypothetical two impacts might have locally thinned the lithosphere resulting in the nearly complete isostatic compensation of the basin.

[22] From the lithospheric thicknesses that best explain the isostatic compensation states in Figure 3c, we classified the mascons >400 km in diameter into three groups. The thickness does not seem to depend much on the ages, but more on the locations as shown in Figure 2 (i.e., mascons of the same group are close to one another). In Figure 2, relatively young volcanic complexes such as the Marius Hills (12°N, 51°W) and the Aristarchus Plateau (25°N, 50°W) are shown as well (blue circles). Positive gravity anomalies of such volcanic complexes might indicate the existence of heavy mare basalts down to a certain depth rather than mantle plugs that characterize the positive gravity anomalies of mascons. Both the group A mascons ($T_e < 20$ km) and the volcanic complexes are in the Oceanus Procellarum region, suggesting a certain thermal anomaly may have existed there.

[23] From a numerical modeling of thermochemical convection, *Zhong et al.* [2000] proposed that uplift of a single plume caused by the existence of a relatively small core may explain hemispheric asymmetry of mare basalts. It may also have something to do with the thermal anomaly in the Oceanus Procellarum region. Future gravimetric studies of the lunar farside in the SELENE (Selenological and Engineering Explorer) relay satellite mission would certainly provide another clue to elucidate the origin of the near- and farside dichotomy in the lunar evolution [*Matsumoto et al.*, 2002].

[24] **Acknowledgments.** This study was carried out while the authors were at the Mizusawa Astrogeodynamic Observatory, National Astronomical Observatory, Japan. Gravity and topography data used in this study are provided by NASA Planetary Data System Geosciences Node (<http://www.pds.wustl.edu>). Constructive comments by two anonymous reviewers improved quality of the paper.

References

- Arkani-Hamed, J. (1998), The lunar mascons revisited, *J. Geophys. Res.*, *103*, 3709–3739.
- Binder, A. B. (1998), Lunar Prospector: Overview, *Science*, *281*, 1475–1476.
- Dehon, R. A., and J. D. Waskom (1976), Geologic structure of the eastern mare basins, *Proc. Lunar Planet. Sci. Conf. 7th*, 2729–2746.
- Kaula, W. M. (1963), The investigation of the gravitational fields of the Moon and planets with artificial satellites, *Adv. Space Sci. Technol.*, *5*, 210–230.
- Konopliv, A. S., S. W. Asmar, E. Carranza, W. L. Sjogren, and D. N. Yuan (2001), Recent gravity models as a result of the Lunar Prospector mission, *Icarus*, *150*, 1–18.
- Matsumoto, K., K. Heki, and H. Hanada (2002), Global lunar gravity field recovery from SELENE, paper presented at IVS 2002 General Meeting, Int. VLBI Serv. for Geod. and Astrometry, Tsukuba, Japan.
- Neumann, G. A., M. T. Zuber, D. E. Smith, and F. G. Lemoine (1996), The lunar crust: Global structure and signature of major basins, *J. Geophys. Res.*, *101*, 16,841–16,864.
- Parker, R. L. (1972), The rapid calculation of potential anomalies, *Geophys. J. R. Astron. Soc.*, *31*, 447–455.
- Reindler, L., and J. Arkani-Hamed (2001), The compensation state of intermediate size lunar craters, *Icarus*, *153*, 71–88.
- Scott, D. H. (1974), The geologic significance of some lunar gravity anomalies, *Proc. Lunar Planet. Sci. Conf. 5th*, 3025–3036.
- Smith, D. E., M. T. Zuber, G. A. Neumann, and F. G. Lemoine (1997), Topography of the Moon from the Clementine lidar, *J. Geophys. Res.*, *102*, 1591–1611.
- Solomon, S. C., and J. W. Head (1980), Lunar mascon basins lava filling, tectonics, and evolution of the lithosphere, *Rev. Geophys.*, *18*, 107–141.
- Spohn, T., W. Konrad, D. Breuer, and R. Ziethe (2001), The longevity of lunar volcanism: Implications of thermal evolution calculations with 2D and 3D mantle convection models, *Icarus*, *149*, 54–65.
- Stevenson, D. J., T. Spohn, and G. Schubert (1983), Magnetism and thermal evolution of the terrestrial planets, *Icarus*, *54*, 466–489.

- Sugano, T., and K. Heki (2004), High resolution lunar gravity anomaly map from the Lunar Prospector line-of-sight acceleration data, *Earth Planets Space*, *56*, 81–86.
- Turcotte, D. L., R. J. Willemann, W. F. Haxby, and J. Norberry (1981), Role of membrane stresses in the support of planetary topography, *J. Geophys. Res.*, *86*, 3951–3959.
- Wieczorek, M. A., and R. J. Phillips (1998), Potential anomalies on a sphere: Applications to the thickness of the lunar crust, *J. Geophys. Res.*, *103*, 1715–1724.
- Wieczorek, M. A., and R. J. Phillips (1999), Lunar multiring basins and the cratering process, *Icarus*, *139*, 246–259.
- Wieczorek, M. A., and M. T. Zuber (2001), A Serenitatis origin for the Imbrian grooves and South Pole-Aitken thorium anomaly, *J. Geophys. Res.*, *27*, 853–864.
- Williams, K. K., and M. T. Zuber (1996), Re-evaluation of mare thicknesses based on lunar crater depth-diameter relationships, *Proc. Lunar Planet. Sci. Conf. 27th*, 1441–1442.
- Zhong, S., E. M. Parmentier, and M. T. Zuber (2000), A dynamic origin for the global asymmetry of lunar mare basalts, *Earth Planet. Sci. Lett.*, *177*, 131–140.

K. Heki, Division of Earth and Planetary Sciences, Hokkaido University, N10 W8, Kita-ku, Sapporo, Hokkaido 060-0810, Japan. (heki@ep.sci.hokudai.ac.jp)

T. Sugano, Division of Earth and Planetary Sciences, Kyoto University, Oiwake-cho, Kitashirakawa, Sakyo-ku, Kyoto 606-8502, Japan. (sugano@miz.nao.ac.jp)